Supplement of Atmos. Chem. Phys., 23, 9815–9836, 2023
https://doi.org/10.5194/acp-23-9815-2023-supplement

Atmospheric Chemistry and Physics
Open Access

Supplement of

Measurement report: Stoichiometry of dissolved iron and aluminum as an indicator of the factors controlling the fractional solubility of aerosol iron – results of the annual observations of size-fractionated aerosol particles in Japan

Kohei Sakata et al.

Correspondence to: Kohei Sakata (sakata.kohei@nies.go.jp)

1. Supplemental Note: Major ion concentration

1.1. Major ion concentrations

1.1.1. Cations

Sodium ion, Mg^{2+}, and Ca^{2+} were mainly distributed in coarse aerosol particles, accounting for 88.3 %, 84.8 %, and 79.3 % of the ions in TSP, respectively (Figs. 2a–2c). Sodium ion in aerosol particles was mainly associated with sea spray aerosol (SSA). Magnesium ion was mainly derived from SSA considering that nss-Mg^{2+} accounted for 26.2 ± 22.4 % of the total Mg^{2+}. By contrast, almost all Ca^{2+} (90.8 ± 9.45 %) was present in the form of nss-Ca^{2+}. Calcium ion concentration was higher in spring (March to May) than in other seasons and during Asian dust events (Fig. 2b). A large amount of Asian dust is transported from the Gobi or Taklamakan Deserts in spring (Uematsu et al., 1983; Sullivan et al., 2007a). Therefore, the high Ca^{2+} concentration in spring was attributed to Asian dust. Potassium ion and NH_4^+ were mainly distributed in fine aerosol particles, which accounted for 68.2 ± 9.69 % and 83.0 ± 3.49 % of the ions in TSP, respectively (Figs. 2d and 2e). More than 90 % of K^+ in fine aerosol particles (annual average: 94.5 ± 14.8 %) was present in the form of nss-K^+. The nss-K^+ in fine aerosol particles is mainly derived from either biomass burning or coal combustion (Echalar et al., 1995; Simoneit et al., 2002; Yu et al., 2018). The discussion on the size and seasonal variation of NH_4^+ with NO_3^- and SO_4^{2-} is provided in the next section.

1.1.2. Anions

Chloride ion dominated in coarse aerosol particles, which contributed 79.5 ± 14.1 % of Cl^- in TSP (Fig. 2f). SSA is the dominant source of Cl^- in aerosol particles. However, the Cl^-/Na^+ mass ratio of aerosol particles was not identical to that of seawater (Fig. S3a). Chloride ion concentration in coarse aerosol particles was depleted relative to the expected Cl^- concentration in non-aged SSA (= $Na^+_{aerosol} \times [Cl^-/Na^+]_{seawater}$), and the depletion ratio of Cl^- in coarse aerosol particles to Cl^- in non-aged SSA was 34.7% ± 28.2%. Cl^- depletion was caused by the chemical reaction of NaCl with HNO_3 and H_2SO_4 as follows (Finlayson-Pitts, 2003):

$$NaCl + HNO_3 \rightarrow NaNO_3 + HCl(g), \text{ (R1)}$$

$$2NaCl + H_2SO_4 \rightarrow Na_2SO_4 + 2HCl\ (g). \text{ (R2)}$$

The frequent enrichment of Cl^- in fine aerosol particles relative to that in non-aged SSA (Fig. S3a) and in contrast to that in coarse aerosol particles indicated that emission sources other than SSA contributed to Cl^- in fine aerosol particles. Cl^- enrichment was observed in aerosol samples collected in winter and spring when air masses mainly originated from East Asia (Fig. S1 and S3a). Previous studies have reported that anthropogenic emissions (e.g., coal combustion, industrial processes, and MSWI) and biomass burning are the dominant sources of HCl and Cl^- in fine aerosol particles in East Asia (Fu et al., 2018; Liu et al., 2018). Indeed, the correlation of excess Cl^- concentration (= $-1 \times Cl^-$ loss) with nss-K^+ is a tracer of biomass burning and coal combustion (r: 0.570). In addition, pre-existing particles, including $CaCO_3$ in mineral dust, act as the sink of Cl species (Sullivan et al., 2007b; Tobo et al., 2010). Therefore, the enrichment of Cl^- in fine aerosol particles was caused by the uptake of anthropogenic Cl^- by pre-existing particles.

Sulfate ions and NH_4^+ were mainly distributed in fine aerosol particles (Figs. 2e and 2g) and accounted for 75.8 ± 11.1 % and 88.8 ± 7.68 % of the total anions and cations in fine aerosol particles, respectively. The average fraction of nss-SO_4^{2-} to total SO_4^{2-} (nss-SO_4^{2-}/total SO_4^{2-}) in coarse and fine aerosol particles were 70.1 ± 23.1 % and 99.3 ± 1.44 %, respectively. Thus, nss-SO_4^{2-} was dominant in coarse and fine aerosol particles. Ammonium ion concentration had a good correlation with but was higher than nss-SO_4^{2-} concentration (Fig. S3b). This result indicated that ammonium salts other than $(NH_4)_2SO_4$ and NH_4HSO_4 were present in fine aerosol particles. Ammonium ion concentration was found to have an excellent correlation

with 2 × [nss-SO_4^{2-}] + [NO_3^-] in fine aerosol particles (Fig. S3c). The slope of the regression line was 0.965, indicating that $(NH_4)_2SO_4$ and NH_4NO_3 were the dominant major ion components in fine aerosol particles.

Nitrate ion had concentration peaks not only in fine aerosol particles but also in coarse aerosol particles (Fig. 2h). The average fractions of NO_3^- in coarse and fine aerosol particles in TSP were 61.3 ± 12.3 % and 36.9 ± 10.5 %, respectively. As previously mentioned, NO_3^- in coarse aerosol particles was derived from Cl^- depletion as described in R1. Assuming that NO_3^- caused the depletion of all Cl from SSA in coarse aerosol particles, SSA-associated NO_3^- accounted for only 35.1 ± 25.1 % of NO_3^- in coarse aerosol particles. Therefore, NO_3^- ions were mainly present in coarse aerosol particles other than SSA (non-SSA-NO_3^-). Previous studies have reported that mineral dust is the dominant driver of NO_3^- concentration in coarse aerosol particles (Karydis et al., 2016, Kakavas et al., 2021). In fact, the good correlation between nss-Ca^{2+} and non-SSA-NO_3^- (= total NO_3^- − Cl depletion) found in our coarse aerosol particles (Fig. S3d) indicated that non-SSA-NO_3^- was present in coarse aerosol particles in the form of $Ca(NO_3)_2$. However, our previous study identified gypsum ($CaSO_4 \cdot 2H_2O$) rather than $Ca(NO_3)_2$ as the dominant secondary Ca species in coarse aerosol particles collected in January, November, and the Asian dust event (Miyamoto et al., 2020). Recent studies have demonstrated that hygroscopic $Ca(NO_3)_2$ on the surfaces of mineral dust reacted with $(NH_4)_2SO_4$, resulting in the formation of NH_4NO_3 and $CaSO_4 \cdot 2H_2O$ (Wu et al., 2019, 2020). Thus, NO_3^- taken up in the reaction with $CaCO_3$ is considered to exist in the form of NH_4NO_3 instead of $Ca(NO_3)_2$.

Supplemental Figures

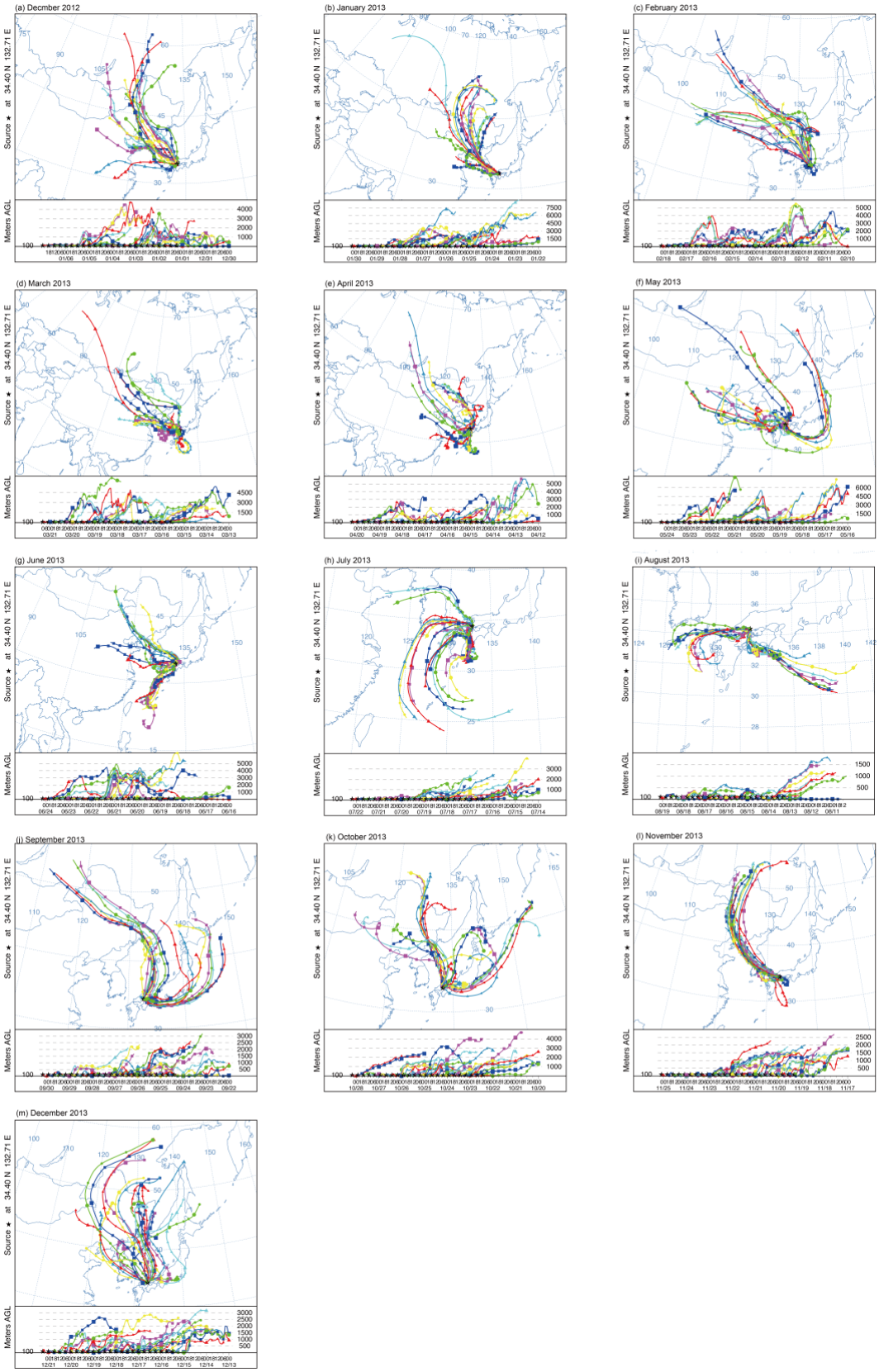

Figure S1: Backward trajectories of sampling periods of (a) December 2012, (b-m) January to December 2013.

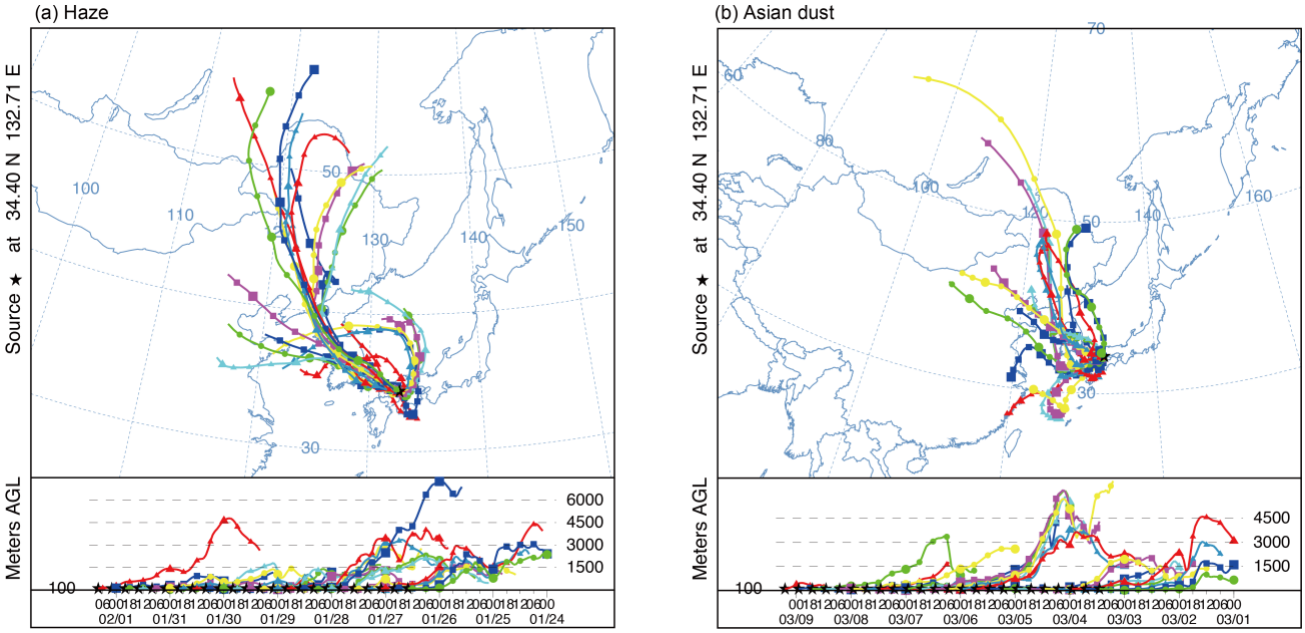

Figure S2: Backward trajectories of sampling periods of (a) Haze and (b) Asian dust events.

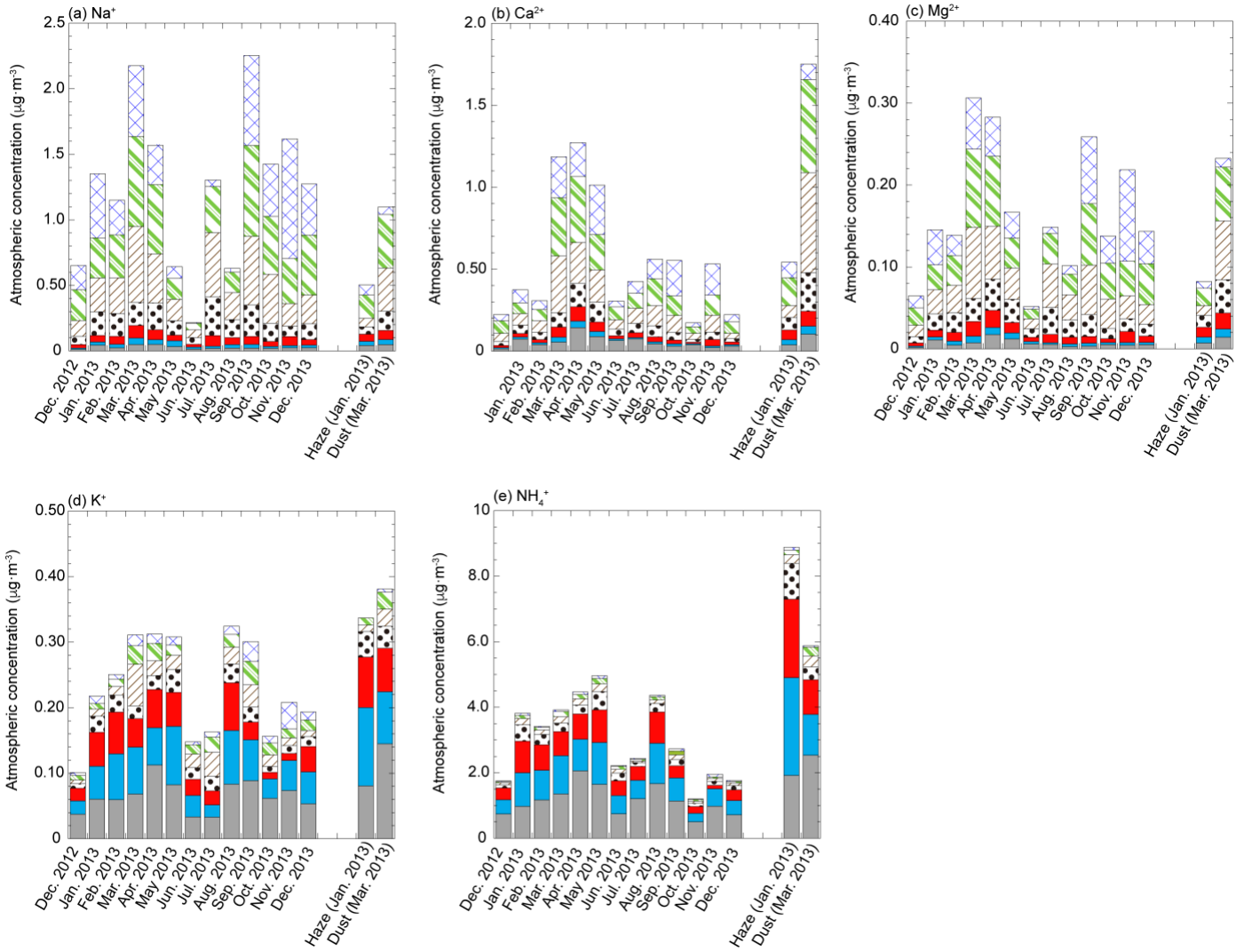

Figure S3: Monthly variations and size distributions of (a) Na^+, (b) Ca^{2+}, (c) Mg^{2+}, (d) K^+, and (e) NH_4^+, (f) Cl−, (g) NO3−, (h) SO42−, and (i) nss-SO42−. The summation of all fractions corresponds to TSP concentration.

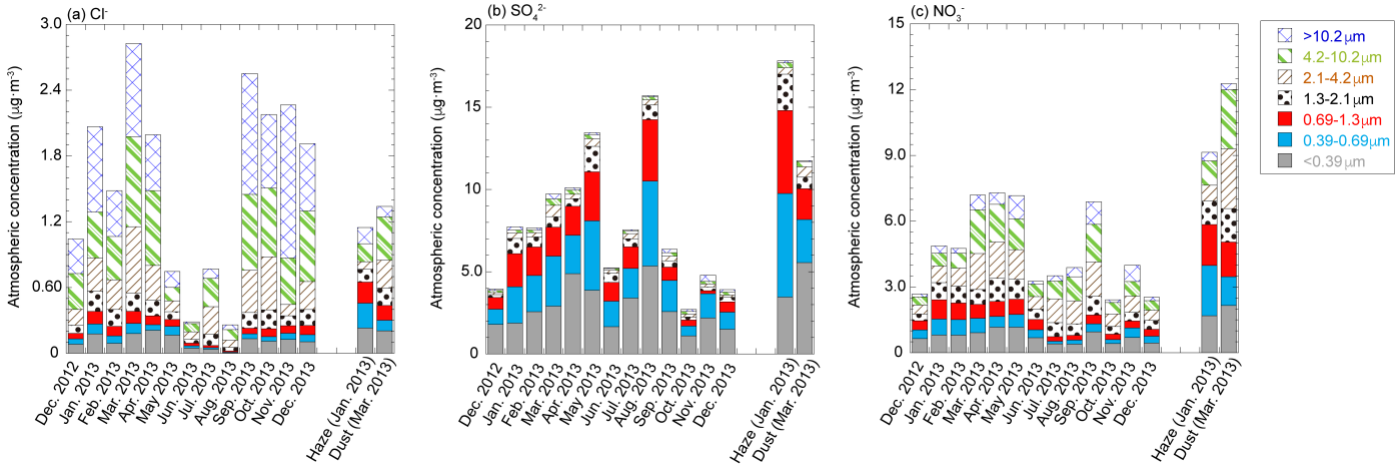

Figure S4: Monthly variations and size distributions of (a) Cl^-, (b) SO_4^{2-}, and (c) NO_3^-. The summation of all fractions corresponds to TSP concentration.

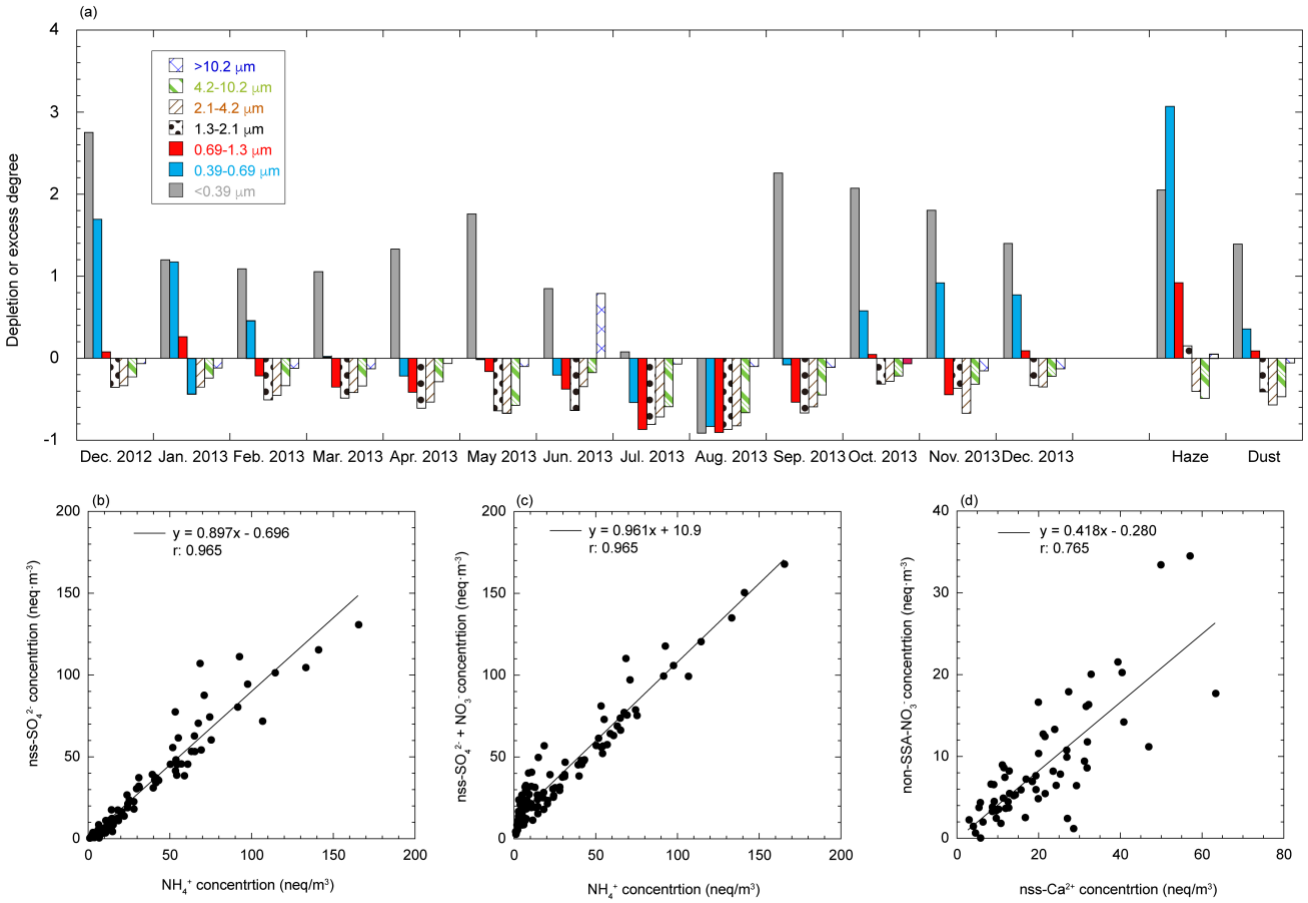

Figure S5: (a) Depletion and excess degree of Cl- in aerosol particles. Depletion or excess degree was calculated by $\frac{(Cl^-/Na^+)_{aerosol}}{(Cl^-/Na^+)_{seawater}} - 1$. (b and c) scatter plots of [NH_4^+] concentration with [nss-SO_4^{2-}] and [nss-SO_4^{2-}]+[NO_3^-]. (d) A scatter plot between [nss-Ca^{2+}] and [non-SSA-NO_3^-].

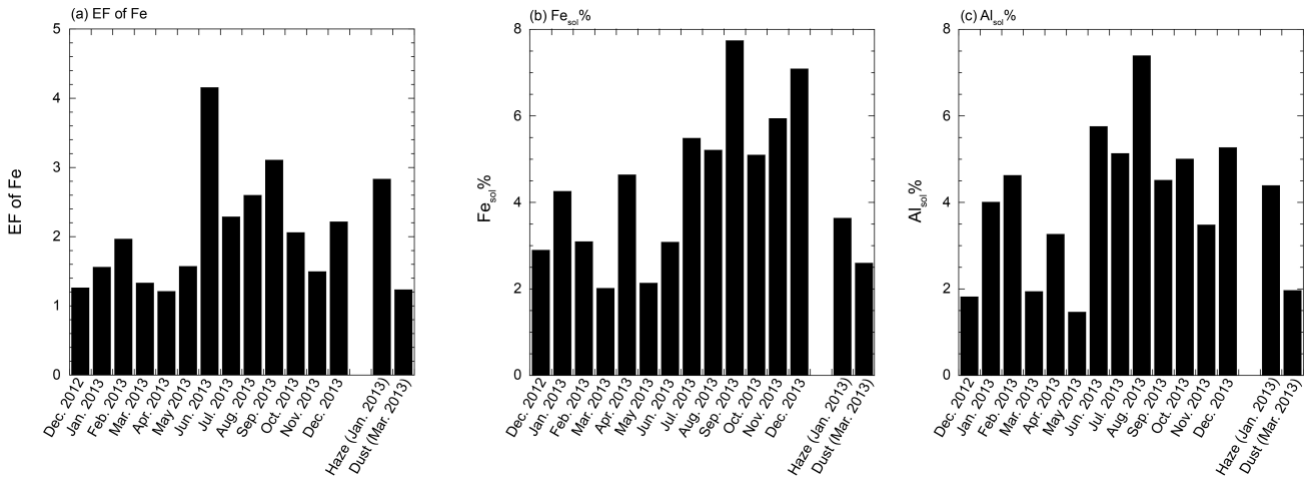

Figure S6: Monthly variations of (a) EF of Fe, (b) Fe_{sol}%, and (c) Al_{sol}% in TSP.

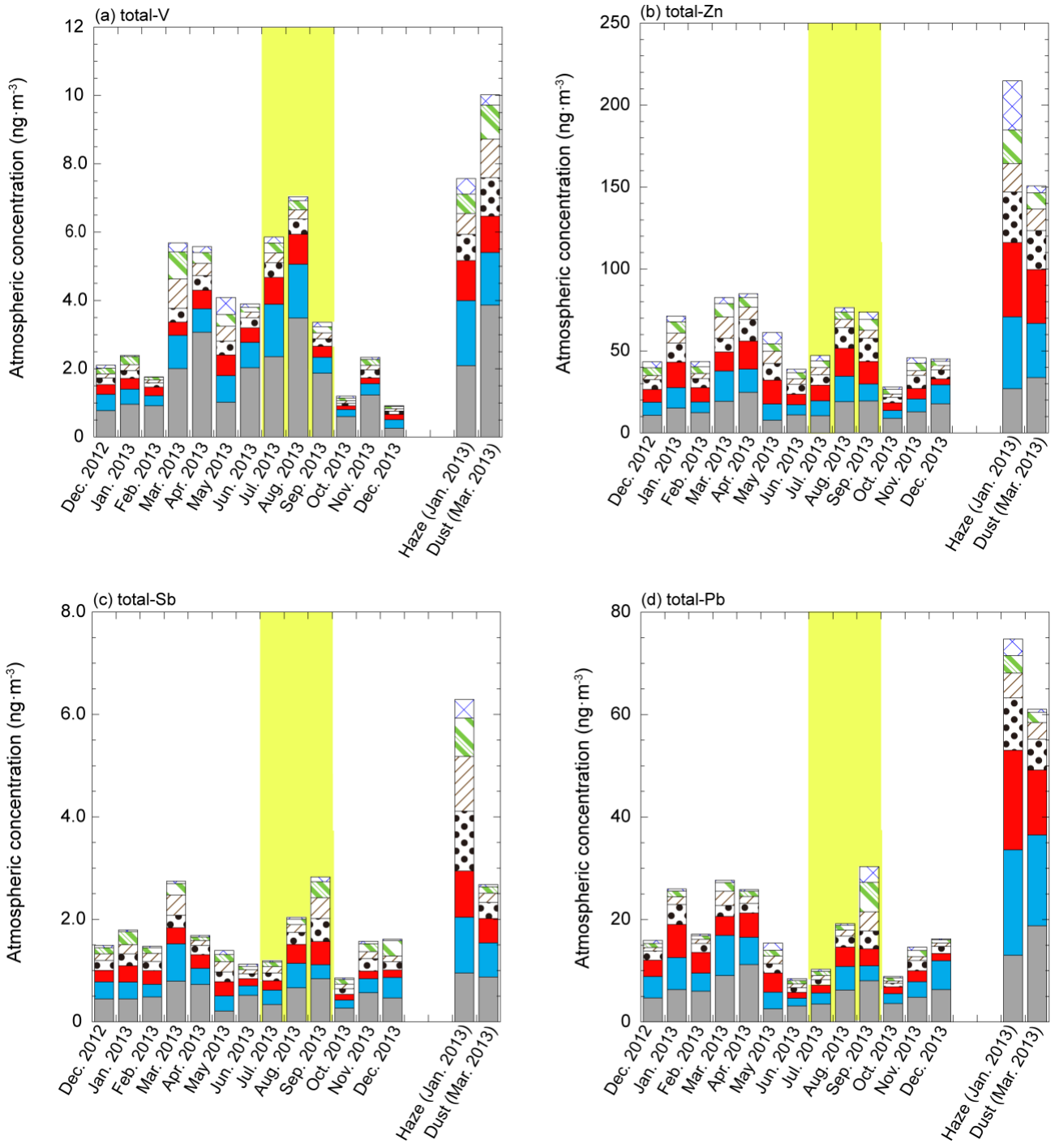

Figure S7: Monthly variation of (a) V, (b) Zn, (c) Sb, and (d) Pb concentrations in size-fractionated aerosol particles. Yellow shaded region shows the sampling period when air mass was derived from the Seto Inland Sea.

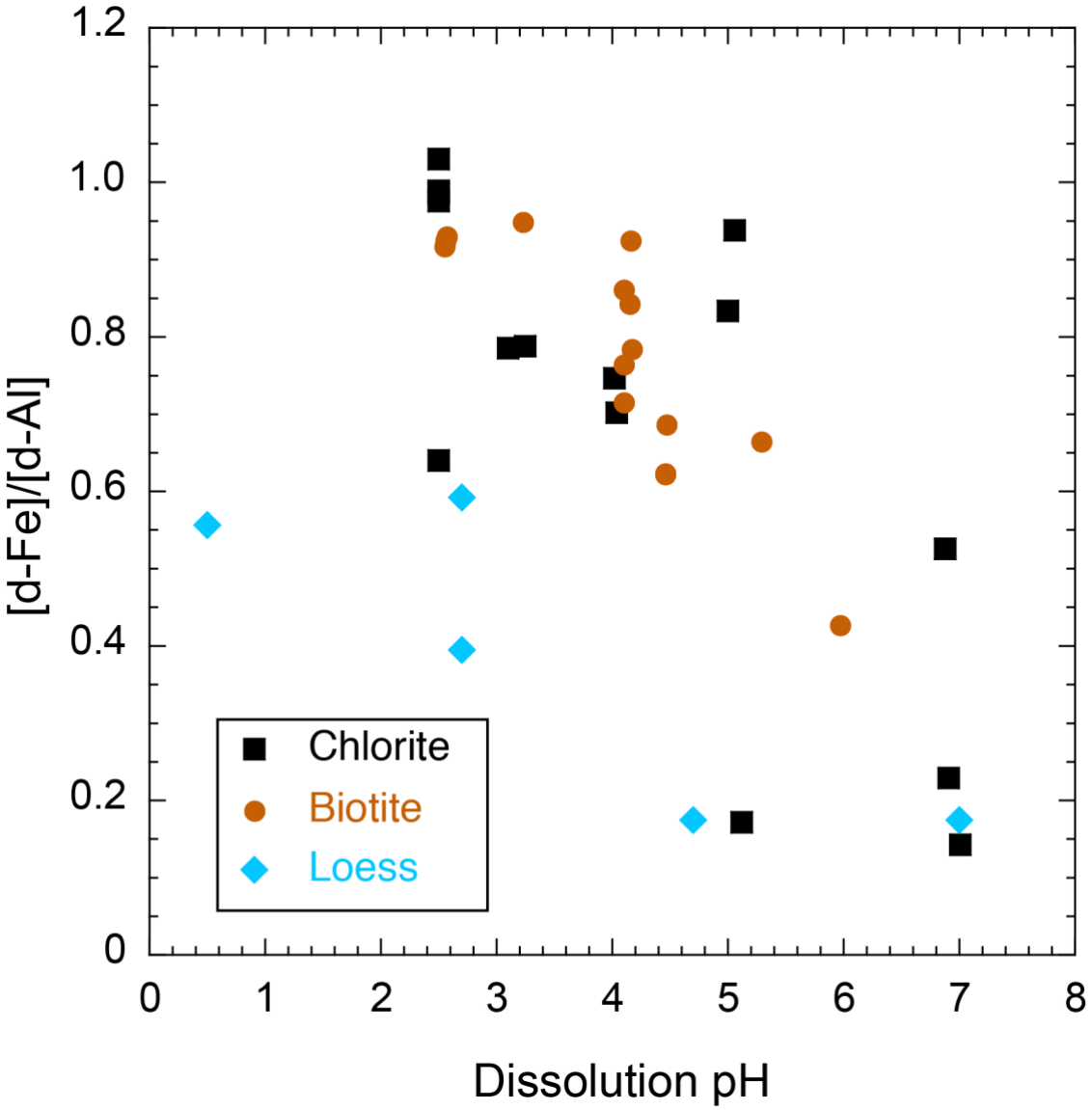

Figure S8: pH dependence of [d-Fe]/[d-Al] ratio of aluminosilicate and loess during proton-promoted dissolution. These [d-Fe]/[d-Al] ratios were referred from Kodama and Schnitzer (1973), Desboeufs et al. (2001), Lowson et al. (2005), and Bray et al. (2015).

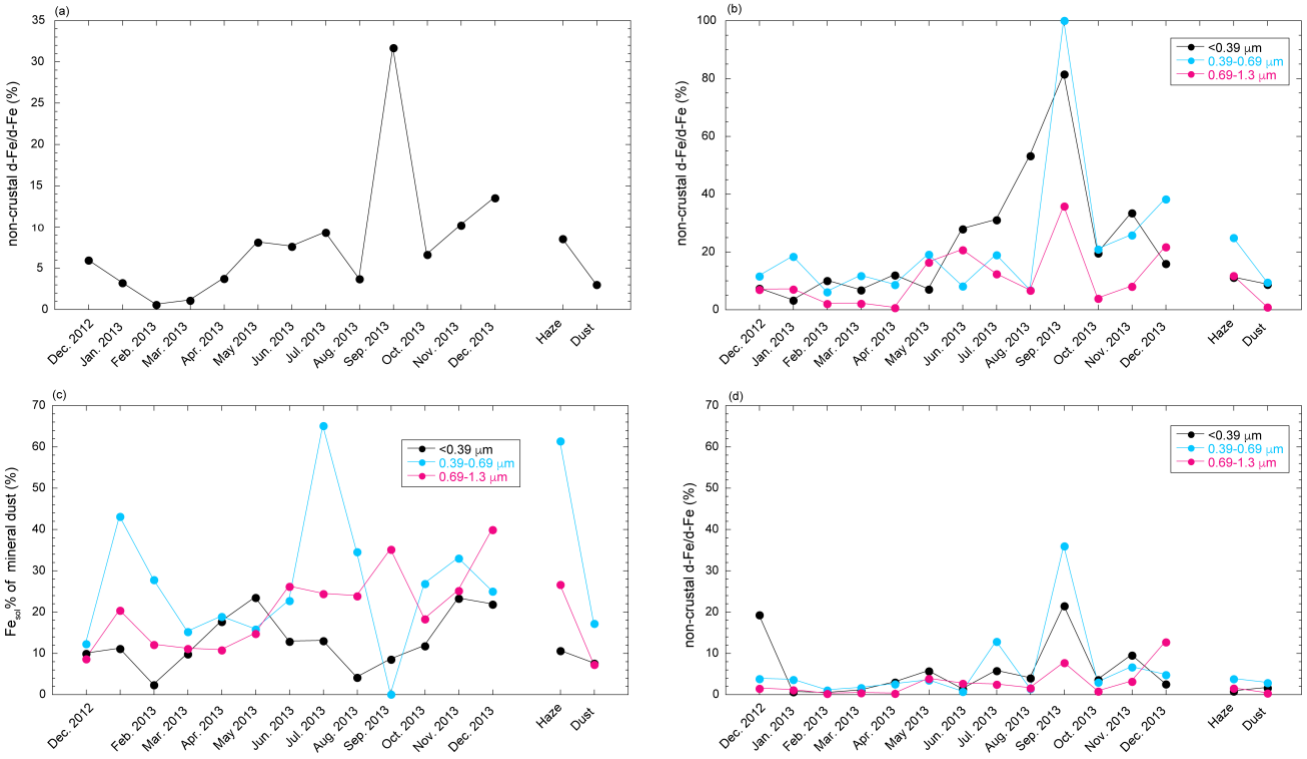

Figure S9: Relative abundance of pyrogenic Fe to d-Fe in (a) TSP and (b) fine aerosol particles when [d-Fe]/[d-Al] ratio of non-crustal Fe is 4.67. (c) crustal Fe and (d) pyrogenic Fe when [d-Fe]/[d-Al] ratio of pyrogenic Fe.

Table S1 Sampling information for each sapling period.

Sample name	Sampling period		Total flow
	Start	End	m^3
	Non-dust event		
December 2012	11:30, 25 Dec. 2012	9:20, 7 Jan. 2013	11699.5
January 2013	10:40, 21 Jan. 2013	13:29, 30 Jan. 2013	7624.5
February 2013	10:31 4 Feb. 2013	10:52, 18 Feb. 2013	11740.6
March 2013	17:20, 21 Mar. 2013	17:20, 21 Mar. 2013	9850.1
April 2013	11:38, 8 Apr. 2013	14:30, 20 Apr. 2013	9494.7
May 2013	13:45, 13 May, 2013	14:52, 24 May, 2013	9282.3
June 2013	15:00, 11 Jun. 2013	12:16, 24 Jun. 2013	11477.6
July 2013	14:25, 8 Jul. 2013	13:00, 22 Jul. 2013	11461.2
August 2013	11:45, 6 Aug. 2013	11:25, 19 Aug. 2013	11490.1
September 2013	16:25, 17 Sep. 2013	12:40, 30 Sep. 2013	11386.3
October 2013	14:40, 15 Oct. 2013	13:10, 28 Oct. 2013	11544.3
November 2013	10:45, 12 Nov. 2013	11:05, 25 Nov. 2013	11698.3
December 2013	9:30, 7 Dec. 2013	14:40, 21 Dec. 2013	11838.8
	Dust events		
Haze	14:19, 31 Jan. 2013	17:09, 1 Feb. 2013	936.8
Dust	10:30, 4 Mar. 2013	14:30, 9 Mar. 2013	4840.2

Table S2. Pearson's correlation matrix of non-crustal Fe with trace metal concentrations in coarse aerosol particles.

	non-crust Fe	V	Cu	Zn	Cd	Sb	Pb
non-crust Fe	1.000						
V	0.387	1.000					
Cu	0.747	0.553	1.000				
Zn	0.586	0.692	0.794	1.000			
Cd	0.383	0.489	0.548	0.721	1.000		
Sb	0.563	0.449	0.858	0.759	0.700	1.000	
Pb	0.457	0.568	0.677	0.813	0.929	0.820	1.000

Table S3 Pearson's correlation matrix of non-crustal Fe with trace etals in fine aerosol particles.

	non-crustal Fe	V	Cu	Zn	Cd	Sb	Pb
non-crustal Fe	1.000						
V	0.601	1.000					
Cu	0.725	0.649	1.000				
Zn	0.795	0.555	0.911	1.000			
Cd	0.850	0.596	0.853	0.923	1.000		
Sb	0.807	0.741	0.799	0.821	0.887	1.000	
Pb	0.765	0.555	0.880	0.947	0.956	0.827	1.000

References

Bray, A. W., Oelkers, E. H., Bonneville, S., Wolff-Boenisch, D., Potts, N. J., Fones, G., and Benning, L. G.: The effect of pH, grain size, and organic ligands on biotite weathering rates, Geochim. Cosmochim. Acta, 164, 127–145, http://dx.doi.org/10.1016/j.gca.2015.04.048, 2015.

Desboeufs, K. V., Losno, R., Colin, J. L.: Factors influencing aerosol solubility during cloud processes, Atmos. Environ., 35, 3529–3537, https://doi.org/10.1016/S1352-2310(00)00472-6, 2001.

Kodama, H., Schnitzer, M.: Dissolution of chlorite minerals by fulvic acid, Can. J. Soil Sci., 53, 240–243, https://doi.org/10.4141/cjss73-036, 1973.

Lowson, R. T., Comarmond, J., Rajaratnam, G., Brown, P. L.: The kinetics of the dissolution of chlorite as a function of pH and at 25ºC, Geochim. Cosmochim. Acta, 69, 1687–1699, https://doi.org/10.1016/j.gca.2004.09.028, 2005.

Uematsu, M.; Duce, R. A., Prospero, J. M., Chen, L., Merrill, J. T., McDonald, R. L.: Transport of mineral aerosol from Asia over the north Pacific Ocean. J. Geophys. Res., 88, 5343–5352, https://doi.org/10.1029/JC088iC09p05343, 1983.

Sullivan, R. C., Guazzotti, S. A., Sodeman, D. A., and Prather, K. A.: Direct observations of the atmospheric processing of Asian mineral dust, Atmos. Chem. Phys., 7, 1213–1236, https://doi.org/10.5194/acp-7-1213-2007, 2007a.

Echalar, F., Gaudichet, A., Cachier, H., Artaxo, P.: Aerosol emissions by tropical forest and savanna biomass burning: characteristic trace elements and fluxes. Geophys. Res. Lett., 22, 3039–3042, https://doi.org/10.1029/95GL03170, 1995.

Simoneit, B. R. T.: Biomass burning – a review of organic tracers for smoke from incomplete combustion, Appl. Geochem., 17, 129–162, https://doi.org/10.1016/S0883-2927(01)00061-0, 2002.

Yu, J., Yan, C., Liu, Y., Li, X., Zhou, T., Zheng, M.: Potassium: a tracer for biomass burning in Beijing? Aerosol Air Qual. Res., 18, 2447–2459, https://doi.org/10.4209/aaqr.2017.11.0536, 2018.

Finlayson-Pitts, B. J.: The tropospheric chemistry of sea salt: A molecular-level view of the chemistry of NaCl and NaBr, Chem. Rev., 103, 4801–4822, https://doi.org/10.1021/cr020653t, 2003.

Fu, X., Wang, T., Wang, S., Zhang, L., Cai, S., Xing, J., Hao, J.: Anthropogenic emissions of hydrogen chloride and fine particulate chloride in China, Environ. Sci. Technol., 52, 1644–1654, https://doi.org/10.1021/acs.est.7b05030, 2018.

Liu, Y., Fan, Q., Chen, X., Zhao, J., Ling, Z., Hong, Y., Li, W., Chen, X., Wang, M., Wei, X.: Modeling the impact of chlorine emissions from coal combustion and prescribed waste incineration on tropospheric ozone formation in China, Atmos. Chem. Phys., 18, 2709–2724, https://doi.org/10.5194/acp-18-2709-2018, 2018.

Sullivan, R. C., Guzzotti, S. A., Sodeman, D. A., Tang, Y., Carmichael, G. R. Prather, K. A.: Mineral dust is a sink for chlorine in the marine boundary layer, Atmos. Environ., 41, 7166–7179, https://doi.org/10.1016/j.atmosenv.2007.05.047, 2007b.

Tobo, Y., Zhang, D., Matsuki, A., Iwasaka, Y.: Asian dust particles converted into aqueous droplets under remote marine atmospheric conditions, Proc. Natl. Acad. Sci. U.S.A., 107, 17905–17910, https://doi.org/10.1073/pnas.1008235107, 2010.

Kakavas, S., Patoulias, D., Zakoura, M., Nenes, A., Pandis, S. N.: Size-resolved aerosol pH over Europe during summer, Atmos. Chem. Phys., 21, 799–811, https://doi.org/10.5194/acp-21-799-2021, 2021.

Karydis, V. A., Tsimpidi, A. P., Pozzer, A., Astitha, M., Lelieveld, J.: Effect of mineral dust on global atmospheric nitrate concentrations, Atmos. Chem. Phys., 16, 1491–1509, https://doi.org/10.5194/acp-16-1491-2016, 2016.

Miyamoto, C., Sakata, K., Yamakawa, Y., and Takahashi, Y.: Determination of calcium and sulfate species in aerosols associated with the conversion of its species through reaction processes in the atmosphere and its influence on cloud condensation nuclie activation. Atmos. Environ., 223, 117193, https://doi.org/10.1016/j.atmosenv.2019.117193, 2020.

Wu, C., Wang, G., Cao, C., Li, J., Li, J., Wu, F., Huang, R., Cao, J., Han, Y., Ge, S., Xie, Y., Xue, G., Wang, X.: Chemical characteristics of airborne particels in Xi'an inland China during dust storm episodes: Implications for heterogeneous formation of ammonium nitrate and enhancement of N-deposition, Environ. Pollut., 244, 877–884, https://doi.org/10.1016/j.envpol.2018.10.019, 2019.

Wu, C., Zhang, G., Wang, G., Lv, S., Li, D., Liu, L., Li, J., Liu, S., Du, W., Meng, J., Qiao, L., Zhou, M., Huang, C., Wang, H.: Efficient heterogeneous formation of ammonium nitrate on the saline mineral particle surface in the atmosphere of East Asia during dust storm periods, Environ. Sci. Technol., 54, 15622–156320, https://dx.doi.org/10.1021/acs.est.0c04544, 2020.